Mathematical Model of the Binding of Allosteric Effectors to the Escherichia coli PII Signal Transduction Protein GInB

ARTICLE *in* BIOCHEMISTRY · MARCH 2013

Impact Factor: 3.02 · DOI: 10.1021/bi301659r · Source: PubMed

6 AUTHORS, INCLUDING:

Thiago André Weschenfelder
Universidade Federal do Paraná
5 PUBLICATIONS **76** CITATIONS
SEE PROFILE

Emanuel M Souza
Universidade Federal do Paraná
249 PUBLICATIONS **2,826** CITATIONS
SEE PROFILE

Luciano Huergo
Universidade Federal do Paraná
55 PUBLICATIONS **541** CITATIONS
SEE PROFILE

David Alexander Mitchell
Universidade Federal do Paraná
164 PUBLICATIONS **3,466** CITATIONS
SEE PROFILE

BIOCHEMISTRY
including biophysical chemistry & molecular biology

Article

pubs.acs.org/biochemistry

Mathematical Model of the Binding of Allosteric Effectors to the *Escherichia coli* PII Signal Transduction Protein GlnB

Ricardo Alves da Rocha,[†] Thiago André Weschenfelder,[‡] Fernanda de Castilhos,[‡,§] Emanuel Maltempi de Souza,[†] Luciano Fernandes Huergo,[†] and David Alexander Mitchell*[,†]

[†]Departamento de Bioquímica e Biologia Molecular, Universidade Federal do Paraná, Cx.P. 19046 Centro Politécnico, Curitiba 81531-980, Paraná, Brazil

[‡]Departamento de Engenharia Química, Universidade Federal do Paraná, Cx.P. 19011 Centro Politécnico, Curitiba 81531-980, Paraná, Brazil

Supporting Information

ABSTRACT: PII proteins are important regulators of nitrogen metabolism in a wide variety of organisms: the binding of the allosteric effectors ATP, ADP, and 2-oxoglutarate (2-OG) to PII proteins affects their ability to interact with target proteins. We modeled the simultaneous binding of ATP, ADP, and 2-OG to one PII protein, namely GlnB of *Escherichia coli*, using a modeling approach that allows the prediction of the proportions of individual binding states. Four models with different binding rules were compared. We selected one of these models (that assumes that the binding of the first nucleotide to GlnB makes it harder for subsequent nucleotides to bind) and used it to explore how physiological concentrations of ATP, ADP, and 2-OG would affect the proportions of those states of GlnB that interact with the target proteins ATase and NtrB. Our simulations indicate that GlnB can, as suggested by previous researchers, act as a sensor of both 2-OG and the ATP:ADP ratio. We conclude that our modeling approach will be an important tool in future studies concerning the PII binding states and their interactions with target proteins.

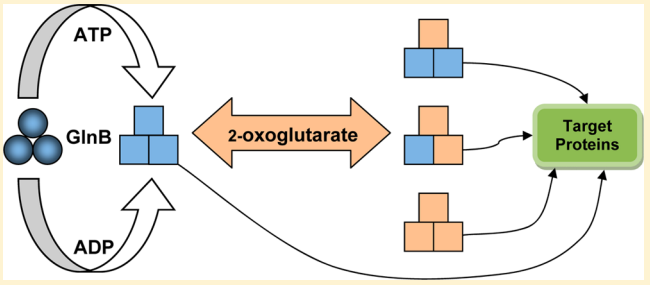

The PII proteins play an important role as regulators of nitrogen metabolism in a wide variety of organisms, including archaea, bacteria, red algae, and plants. These proteins are homotrimers with a mass of around 12 kDa per subunit. Both the three-dimensional structure and the presence of binding sites for the allosteric effectors ATP, ADP, and 2-oxoglutarate (2-OG) are highly conserved within the PII protein family.[1] In fact, all the PII proteins studied to date have three nucleotide binding sites, located in the lateral clefts between the monomers,[2,3] for which ATP and ADP compete for binding.[4−6] Furthermore, PII proteins can bind up to three molecules of 2-OG, one in the vicinity of each ATP binding site. 2-OG binding occurs cooperatively with ATP binding and requires the presence of Mg^{2+}.[7−10]

Two PII proteins are synthesized by *Escherichia coli*, GlnB and GlnK. GlnB is the major regulator of ammonium assimilation.[11−14] Under conditions of nitrogen sufficiency, it interacts with ATase, with the resulting complex inactivating glutamine synthetase (GS) catalytic subunits by adenylylation. It also interacts with NtrB, with the resulting complex promoting dephosphorylation of NtrC and thereby reducing the level of expression of GS.[6] On the other hand, GlnK is dedicated to the control of ammonium flux through the ammonium transporter AmtB.[15]

The ability of GlnB to interact with ATase or NtrB is determined by its "binding state", namely the particular combination of effectors that is bound to it.[4,16] A mathematical model that is capable of predicting how the binding state of GlnB is determined by the intracellular concentrations of ATP, ADP, and 2-OG would be a useful tool for understanding how GlnB functions to control nitrogen metabolism under varying physiological conditions. Two mathematical models have already been proposed to describe the binding of effectors to *E. coli* GlnB, but both have limitations. The model of Bruggeman et al.[17] assumes that GlnB is always saturated with ATP and that the first, second, and third molecules of 2-OG bind with different affinities. Their model does not recognize that ADP is always present in the cell and competes with ATP for binding to GlnB. Because it does not describe the binding of ATP, its application is limited to situations in which the ATP concentration is saturating. The model of Jiang and Ninfa[6] involves the application of an equation for the binding of a single effector to each of three different data sets: ATP as the only effector present, ADP as the only effector present, and both ATP and 2-OG present as effectors. For each data set, they selected a binding equation that considered an appropriate number of classes of sites (i.e., allowing for different affinities for subsequent bindings of the effector): three classes for ATP,

Received: December 13, 2012
Revised: March 9, 2013
Published: March 21, 2013

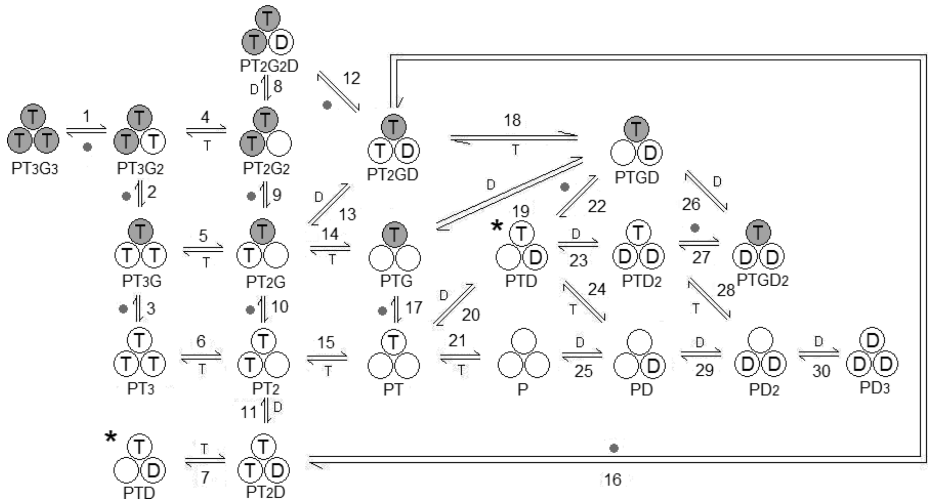

Figure 1. Representation of the system that was modeled. There are a total of 30 reversible dissociation reactions (but only 15 for M2) and 20 possible PII states (but only 13 for M2). Symbols: P, PII protein; T, ATP; D, ADP; G and (shaded circle), 2-oxoglutarate. Shaded monomers also have 2-oxoglutarate bound to them. The state with marked with an asterisk is shown twice in the scheme to avoid crossover of the arrows representing the reactions.

one class for ADP, and three classes for 2-OG in the presence of saturating concentrations of ATP. However, because in each case they considered only a single effector, their equations cannot be used to predict the competitive binding of ATP and ADP when both are present.

In summary, neither of the two models described to date has the flexibility to describe the states of GlnB when ATP, ADP, and 2-OG are present simultaneously. The aim of this work was to develop a model for GlnB of *E. coli* that has this flexibility. Experimental data obtained by Jiang and Ninfa[6] were used for both estimation of the model parameters and validation of the model. The model was applied to predict how fluctuations of ATP, ADP, and 2-OG can alter the binding states of GlnB in vivo.

MODEL DEVELOPMENT

Model Structure. Before we present the models, it is important to consider the state of the ATP molecules in the system. Structural evidence obtained with PII proteins from *Azospirillum brasilense*, *Synechococcus elongatus*, and *Achaeoglobus fulgidus* has shown that the binding of 2-OG requires Mg^{2+}, with this ion being coordinated between the 2-OG and the phosphate groups of the ATP.[7,8,10] Therefore, the availability of Mg^{2+} could potentially be a limiting factor in the binding of 2-OG to PII proteins. The K_d of the reaction Mg-ATP → Mg^{2+} + ATP is 0.0603 mM.[18] Because the free Mg^{2+} concentration in the cytoplasm of *E. coli* is at least 1 mM,[19] this means that at least 94% of the ATP is in the form of Mg-ATP when the "ATP + Mg-ATP" concentration is 1 mM. In their experiments, Jiang and Ninfa[6] used 10 mM Mg^{2+} and up to 1 mM ATP. These conditions ensure that more than 99% of the ATP is in the form of Mg-ATP. On the basis of these considerations, from this point on, we write "ATP" to represent "Mg-ATP".

Although it has been suggested that ATP and ADP can bind to the same trimer,[6,7] it is not clear how the successive binding of ATP and ADP affects the GlnB conformation when both effectors are present, so four different models were constructed. In all four models, each subunit of the trimer has a binding site for which ATP and ADP compete.[6] If (and only if) ATP binds, then it creates a 2-OG binding site on the subunit to which ATP is bound.[7] GlnB can therefore bind three molecules of 2-OG in the presence of ATP. We assumed that 2-OG cannot bind to a GlnB subunit that is occupied by ADP.[7] This leads to a total of 20 possible GlnB states and 30 reversible dissociation reactions (Figure 1). Each state of GlnB is represented by the letter P (symbolizing the GlnB trimer), followed by letters indicating the bound effectors (T for ATP, D for ADP, and G for 2-OG), with subscripts indicating their number per trimer. Each dissociation reaction, involving a particular effector X, is characterized by a dissociation constant, denoted by K_{XN}:

$$K_{XN} = \frac{[X][PX_{N-1}]}{[PX_N]} \quad (1)$$

where [X] is the concentration of the effector in question (i.e., ATP, ADP, or 2-OG), $[PX_N]$ is the concentration of GlnB ,and $[PX_{N-1}]$ is the concentration of the GlnB−effector complex. The number N in the subscript denotes how many effector molecules of that type are present in the complex that dissociates (i.e., N = 1, 2, or 3). The expressions for the dissociation constants of the four models, constructed using the logic of eq 1, are listed in Table S1 of the Supporting Information.

Because GlnB exhibits strong negative cooperativity for binding of subsequent 2-OG molecules,[6,20] all four models assume that the bindings of the first, second, and third 2-OG molecules to the trimer are governed by different dissociation constants (i.e., $K_{G1} \neq K_{G2} \neq K_{G3}$). The binding of 2-OG to a subunit is assumed not to affect the binding of ATP or ADP to adjacent subunits. The four models differ in how they treat the binding of subsequent molecules of ATP or ADP.

Model 1 (M1) is based on the data fitting done by Jiang and Ninfa[6] and considers three classes of binding sites for ATP (i.e., $K_{T1} \neq K_{T2} \neq K_{T3}$) and only one class of binding sites for ADP (i.e., all dissociation constants are characterized by K_{D1}). This means that the binding of ADP does not affect the binding of subsequent molecules of either ATP or ADP and that the binding of ATP affects only the binding of subsequent ATP molecules. These effectors can bind to the same trimer, competing for the same binding sites.

dx.doi.org/10.1021/bi301659r | *Biochemistry* 2013, 52, 2683−2693

Model 2 (M2) assumes that there are two classes of sites both for ATP and for ADP and that these effectors cannot bind to the same trimer. After the binding of the first ATP or ADP, the affinities change, such that $K_{T1} \neq K_{T2}$ and $K_{D1} \neq K_{D2}$. Binding of the second and third ATP or ADP has the same affinity, such that $K_{T2} = K_{T3}$ and $K_{D2} = K_{D3}$.

Model 3 (M3) has the same considerations as M2 but allows ADP and ATP to bind to the same trimer.

Model 4 (M4) assumes that there are three classes of sites to which ATP or ADP can bind, with these effectors being able to bind to the same trimer. After the binding of each nucleotide, the protein changes its affinity for the binding of subsequent nucleotides, such that $K_{T1} \neq K_{T2} \neq K_{T3}$ and $K_{D1} \neq K_{D2} \neq K_{D3}$.

Equations for Bound Ligands. The total concentration of GlnB in the system, represented by $[P]_T$, is equal to the sum of all the binding states:

$$[P]_T = [P] + [PT] + [PTD] + [PTD_2] + [PTG] + [PTGD] + [PTGD_2] + [PT_2] + [PT_2D] + [PT_2G] + [PT_2G_2] + [PT_2GD] + [PT_2G_2D] + [PT_3] + [PT_3G] + [PT_3G_2] + [PT_3G_3] + [PD] + [PD_2] + [PD_3] \quad (2)$$

The concentrations of bound ATP, bound ADP, and bound 2-OG ($[T]_B$, $[D]_B$, and $[G]_B$, respectively) are given by

$$[T]_B = [PT] + [PTD] + [PTD_2] + [PTG] + [PTGD] + [PTGD_2] + 2([PT_2] + [PT_2D] + [PT_2G] + [PT_2G_2] + [PT_2GD] + [PT_2G_2D]) + 3([PT_3] + [PT_3G] + [PT_3G_2] + [PT_3G_3]) \quad (3a)$$

$$[D]_B = [PD] + [PTD] + [PT_2D] + [PTGD] + [PT_2GD] + [PT_2G_2D] + 2([PD_2] + [PTD_2] + [PTGD_2]) + 3[PD_3] \quad (3b)$$

$$[G]_B = [PTG] + [PT_2G] + [PT_3G] + [PTGD] + [PT_2GD] + [PTGD_2] + 2([PT_2G_2] + [PT_3G_2] + [PT_2G_2D]) + 3[PT_3G_3] \quad (3c)$$

For M2, states PTD, PT_2D, PTD_2, PTDG, PT_2GD, and $PTGD_2$ do not exist, and therefore, their concentrations are set to zero.

The average numbers of ATP, ADP, and 2-OG molecules bound to each GlnB trimer (n_{ATP}, n_{ADP}, and $n_{2\text{-}OG}$, respectively) are given by

$$n_{ATP} = \frac{[T]_B}{[P]_T} \quad (4a)$$

$$n_{ADP} = \frac{[D]_B}{[P]_T} \quad (4b)$$

$$n_{2\text{-}OG} = \frac{[G]_B}{[P]_T} \quad (4c)$$

All states of GlnB can be written as functions of the concentrations of free ligands (i.e., [T], [D], or [G]), the concentration of GlnB (i.e., [P]), and the dissociation constants. For example, using the dissociation constants for reactions 17 and 21 (Figure 1), it is possible to deduce equations for the concentrations of states PT and PTG:

$$[PT] = \frac{[P][T]}{K_{T1}} \quad (5a)$$

$$[PTG] = \frac{[PT][G]}{K_{G1}} = \frac{\frac{[P][T]}{K_{T1}}[G]}{K_{G1}} = \frac{[P][T][G]}{K_{T1}K_{G1}} \quad (5b)$$

This procedure is repeated for all the states of GlnB in all four models, giving the expressions listed in Table S2 of the Supporting Information. For each model, these expressions are then substituted into eqs 3a−3c, which, in turn, are substituted into eqs 4a−4c. After this, all terms in eqs 4a−4c contain [P], which therefore cancels out. If the total concentrations of the ligands (denoted by $[T]_T$, $[D]_T$, and $[G]_T$ for ATP, ADP, and 2-OG, respectively) are known, then it is possible to replace $[T]_B$ in eq 4a with $[T]_T - [T]$, $[D]_B$ in eq 4b with $[D]_T - [D]$, and $[G]_B$ in eq 4c with $[G]_T - [G]$. After this, eqs 4a−4c represent three nonlinear equations in [T], [D], and [G].

METHODS

Data Gathering. Experimental data for free, bound, and total concentrations of effectors and protein concentrations were extracted from ref 6 [their Figures 9A−E and 10A−D, totaling 61 experimental points (see Table S3 of the Supporting Information)]. Because of an inconsistency in their Figure 9D, where the concentration of bound ADP was higher than the total ADP concentration at low ADP concentrations, we assumed that their *X*-axis was mislabeled, so we used their *X*-axis values as free ADP concentrations rather than total ADP concentrations.

Division of Data into Optimization and Validation Data Sets. Given estimates of the dissociation constants (these estimates being available during the optimization procedure) and the concentrations of free ligands, [T], [D], and [G] (even if they equal zero), it is possible to resolve eqs 4a−4c explicitly (after [P] cancels out). This simplifies the optimization procedure by avoiding the need for implementation of a nonlinear equation solver. Of the 61 data sets extracted from ref 6, 25 data sets contained complete information about the concentrations of the free ligands. Of these, 19 data sets were used for the optimization per se, with six data sets being used for a first validation (Table S3 of the Supporting Information). The data set for the second validation consisted of those data sets that did not contain complete concentration data for all of the ligands.

Optimization Method. For each model, the particle swarm optimization (PSO) algorithm[21,22] was used to find the values for the dissociation constants that minimized the following objective function, using the optimization data set in Table S3 of the Supporting Information:

$$SS = \sum_{i=1}^{6} ([T]_{Bi_M} - [T]_{Bi_E})^2 + \sum_{i=7}^{12} ([D]_{Bi_M} - [D]_{Bi_E})^2 + \sum_{i=13}^{19} ([G]_{Bi_M} - [G]_{Bi_E})^2 \quad (6)$$

where SS is the sum of squares, the subscript *i* represents the *i*th line of data in Table S3 of the Supporting Information, the subscript E denotes the experimental value of Jiang and Ninfa[6]

dx.doi.org/10.1021/bi301659r | *Biochemistry* 2013, 52, 2683−2693

listed in Table S3 of the Supporting Information, and the subscript M denotes the corresponding value predicted by the model.

Particle swarm optimization (PSO) is a relatively new metaheuristic algorithm developed by Eberhart and Kennedy.[21,22] It is a stochastic, derivative-free global optimizer in which a number of particles form a swarm that evolve or fly throughout the problem hyperspace to search for an optimal or a near optimal solution. Each particle has two vectors associated with it: the position vector, which represents a possible solution to the optimization problem, and the velocity vector, which represents the direction and speed with which the particle changes position in successive iterations. During the search, the particles exchange information with each other, leading them to form a swarm that moves toward the global minimum of the objective function.

As with other stochastic algorithms, PSO has key advantages over deterministic derivative-based optimization algorithms.[23] First, it requires only a fitness function to measure the "quality" of a solution, whereas deterministic algorithms require complex mathematical operations like gradient, Hessian, or matrix inversion. Second, because it is a population-based method that uses stochastic transition rules, it has the ability to escape local minima and therefore does not require a good initial guess to determine the global minimum. In comparison, deterministic algorithms that start from a single initial guess can easily become "trapped" within a local minimum and thereby fail to find the global minimum.

In the work presented here, PSO was implemented using a FORTRAN subroutine based on the work of van den Bergh and Engelbrecht.[24] A set of initial guesses for the dissociation constants was obtained using a random-number generating subroutine (Numerical Recipes). As PSO is a stochastic algorithm, the estimates of the dissociation constants listed in Table 1 are the averages of the values obtained in five estimation procedures that were started with different randomly generated initial guesses.

Table 1. Fitted Values of the Dissociation Constants and Relative Errors for the Four Models

	Dissociation Constants[a] (μM)			
	model 1	model 2	model 3	model 4
K_{T1}	46	43	46	51
K_{T2}	159	291	234	121
K_{T3}	699	–[b]	–[b]	621
K_{D1}	30	17	16	18
K_{D2}	–[b]	63	77	42
K_{D3}	–[b]	–[b]	–[b]	215
K_{G1}	10	11	11	11
K_{G2}	142	145	144	143
K_{G3}	5079	5622	6845	5823
	Σ|Relative Error|			
	model 1	model 2	model 3	model 4
optimization	0.927	0.680	0.817	0.713
first validation	0.390	0.379	0.456	0.378
second validation	7.747	9.736	6.367	6.199
total	9.05	10.77	7.66	7.38

[a]The values reported for the dissociation constants represent the average of the results obtained when the PSO algorithm was executed five times with different randomly generated initial guesses. [b]The constant does not exist in the model.

Calculation of the Total Relative Error. For each model, the Broyden method for solving nonlinear equations was implemented in a FORTRAN subroutine[25] and used to solve for [T], [D], and [G] for each data line in Table S3 of the Supporting Information, given the total concentrations ($[T]_T$, $[D]_T$, and $[G]_T$) used in the experiment and the appropriate values of the dissociation constants obtained by the PSO algorithm. This was necessary because eqs 4a–4c are not explicit in [T], [D], and [G] for most experimental data.

$[T]_B$, $[D]_B$, and $[G]_B$ were calculated considering the total effector concentration (listed in Table S3 of the Supporting Information) and the values of [T], [D], and [G] obtained through the Broyden method. To provide a basis for comparing the fits of the various models, the total relative error (TRE) was calculated for each model using the values obtained and the values in the experimental data column (Table S3 of the Supporting Information) through eq 7:

$$\mathrm{TRE} = \sum_{i=1}^{61} \left| \frac{P_i - E_i}{E_i} \right| \tag{7}$$

where E_i is the ith experimental data point and P_i is the corresponding value predicted by the model (see Table S4 of the Supporting Information). The TRE was used as the basis of comparison rather than the sum of squares of the residuals to reduce the penalty that a model incurred for failing to predict a single data point well.

Exploration of the Concentrations of the Binding States of GlnB. The sum of the concentrations of all the GlnB binding states equals the total GlnB protein concentration, and each state has its own equation (Table S2 of the Supporting Information). With the K_d values obtained through the optimization method and the values of the concentrations of the free effectors obtained through the Broyden method, this results in a system of 20 equations and 20 unknown variables (i.e., the concentrations of each of the 20 states). This system was solved using TK Solver version 4.0, and consistent values for the concentrations of all GlnB binding states were obtained.

RESULTS

Parameter Estimation and Model Comparison. Table 1 shows the values of the dissociation constants obtained by fitting the four models to the optimization data set and also the sums of the absolute values of the relative errors for fitting to the three data sets extracted from ref 6, namely, the optimization set, the first validation set, and the second validation set. The relative error sum obtained with the second validation data set is used as the main criterion for model comparison because it is the only set that contains, first, experiments in which there is competition between ATP and ADP and, second, experiments in which all three effectors are present at the same time. Using this criterion, the best models are M3 and M4; M1 and M2 have significantly poorer fits (Table 1).

The major problem with M1, which assumes that there is only one dissociation constant for ADP, is that it overestimates the values of bound ADP when ATP is present (Table S4 of the Supporting Information, lines 56, 57, 60, and 61). This poor fit suggests that the binding of ATP to GlnB makes it harder for ADP to bind to the trimer, possibly through a change in the conformation of the trimer. Likewise, M2, which assumes that ATP and ADP cannot bind to the same trimer, adjusts poorly to the experiments in which there is competition between ATP

and ADP (Table S4 of the Supporting Information). This result suggests that GlnB is able to have both ATP and ADP bound simultaneously.

M3 and M4 adjust well to most of the experimental data. Both models have similar total relative errors and similar relative error sums for the individual data sets (Table 1). In both cases, the largest relative errors occur for the same experimental data (lines 42, 44, 47, and 61 in Table S4 of the Supporting Information). The slightly better fit obtained with M4 (Table S4 of the Supporting Information), which has three dissociation constants for each ligand, occurs because it contains two more fitting parameters than does M3, which has only two dissociation constants for ATP and two for ADP. The literature does not help to distinguish between M3 and M4, because no structural evidence about the binding of subsequent ATP molecules in *E. coli* GlnB is available. It should be noted that Jiang and Ninfa[6] obtained a good fit for the binding of ATP considering either two (as M3 has) or three (as M4 has) dissociation constants.

M1 and M3 were chosen for a point-by-point comparison of the errors. M1 was chosen because it is consistent with the fitting work done by Jiang and Ninfa,[6] which suggested three dissociation constants for ATP and one for ADP. M2 was not considered because it had the worst fit. M3 was chosen because it gave a fit comparable to that of M4, but with fewer parameters.

Although for both M1 and M3 the majority of predicted points fall within ±15% of the experimental value obtained by Jiang and Ninfa[6] (i.e., within a relative error of ±0.15) as shown by Figures 2 and 3, M3 has two advantages. First, M3 has a lower total relative error than does M1, mainly because of its better ability to describe the second validation data set (Table 1). Specifically, M3 predicts bound ADP much better than M1 does (Table S4 of the Supporting Information, lines 54−61). Second, M1 systematically overestimates the bound ADP at low ADP concentrations (the black diamonds are all above the 45° line in Figure 3a and have positive values in Figure 3c). With M3, the errors in the estimation of these same data points are more randomly distributed (the black diamonds fall above and below the 45° line in Figure 3b and have negative and positive values in Figure 3d). For both models, the largest single relative error occurs for the prediction of bound ADP in the experiment in which the 2-OG concentration is ∼20 times higher than the ATP and ADP concentrations (Table S4 of the Supporting Information, line 61). For this data point, the error obtained with M1 (see the point marked with the arrow in Figure 3c) is significantly larger than the error obtained with M3 (see the point marked with the arrow in Figure 3d).

Predictions of Effector Binding to GlnB. Because of its good performance in the analysis described above, M3 was used to show how the type of model developed in this work can be used to explore the binding of ATP, ADP, and 2-OG to GlnB, over physiological concentration ranges that have been reported in *E. coli* for these effectors.

When *E. coli* is not starved, the total ATP concentration remains around 3 mM over a range of different growth conditions and growth rates.[16,26] Under starvation, the ATP concentration initially decreases sharply; however, this slows, and even after several hours, the concentration remains above 0.3 mM.[27] The total ADP concentration ranges from around 0.3 mM under well-fed conditions[16] to 1.1 mM under starvation conditions.[28] The total 2-OG concentration normally

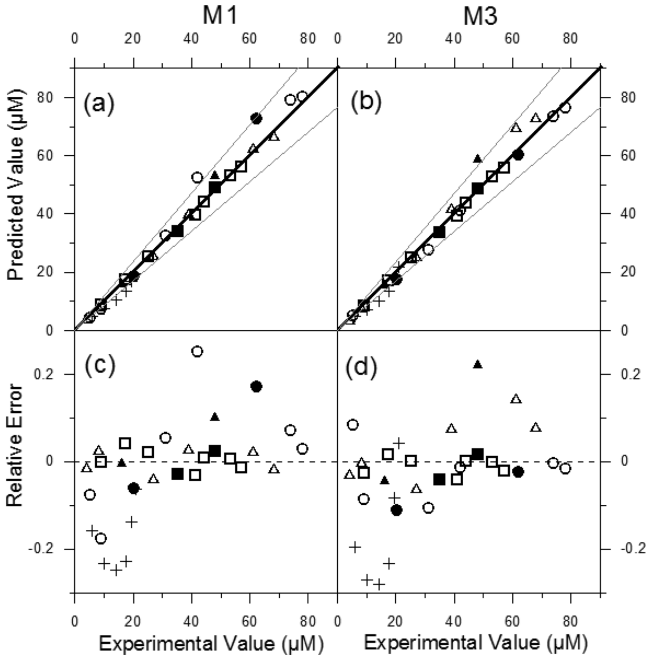

Figure 2. Error analysis of M1 and M3 for higher values. Graphs for M1 are on the left and graphs for M3 on the right. The experimental value and the predicted value represent absolute effector concentrations (micromolar). In graphs a and b, the thick black line represents zero error while the gray lines correspond to ±15% error. Graphs c and d represent the corresponding relative errors, calculated by eq 8. The dashed line in graphs c and d corresponds to zero error. Symbols: (△) ATP optimization data, (○) ADP optimization data, (□) 2-OG optimization data, (▲) ATP first validation data, (●) ADP first validation data, (■) 2-OG first validation data, and (+) ATP second validation data.

varies from 0.1 to 1.4 mM[16,29] but can increase to values above 10 mM during severe nitrogen limitation.[30]

Simulations were conducted using the reported ATP, ADP, and 2-OG concentrations and considering the intracellular GlnB concentration in the micromolar range.[31] In the absence of ADP, 2 mM ATP gives 95% occupation of the nucleotide binding sites of GlnB by ATP (Figure 4a). Added ADP competes with ATP, reducing the extent of ATP binding. Even normal physiological concentrations of ADP (0.3 mM) significantly reduce the amount of ATP bound to GlnB (Figure 4a) (from 95 to 75% at 2 mM ATP, for example). When ATP is absent, 0.3 mM ADP gives around 90% occupation of the nucleotide binding sites of GlnB by ADP (Figure 4b). This analysis suggests that, in vivo, the majority of GlnB proteins will have all three ATP/ADP binding sites occupied.

The presence of 2-OG enhances the binding of ATP. It is important to realize that, according to M3, this is not due to an effect of 2-OG on the values of constants for the binding of ATP to GlnB (i.e., in the model, these values remain unaffected by 2-OG), but rather to the fact that the presence of 2-OG increases the number of states of GlnB to which ATP is bound. There are six states with ATP bound in the absence of 2-OG and 16 states in the presence of 2-OG (Figure 1). When ADP is absent, the enhancement of ATP binding by 2-OG is only slight, except at very low ATP concentrations (Figure 4c). When ADP is present, the enhancement of ATP binding is much greater, especially at lower ATP concentrations (Figure 4d), which is in agreement with prior studies by Jiang and Ninfa.[6]

dx.doi.org/10.1021/bi301659r | *Biochemistry* 2013, 52, 2683−2693

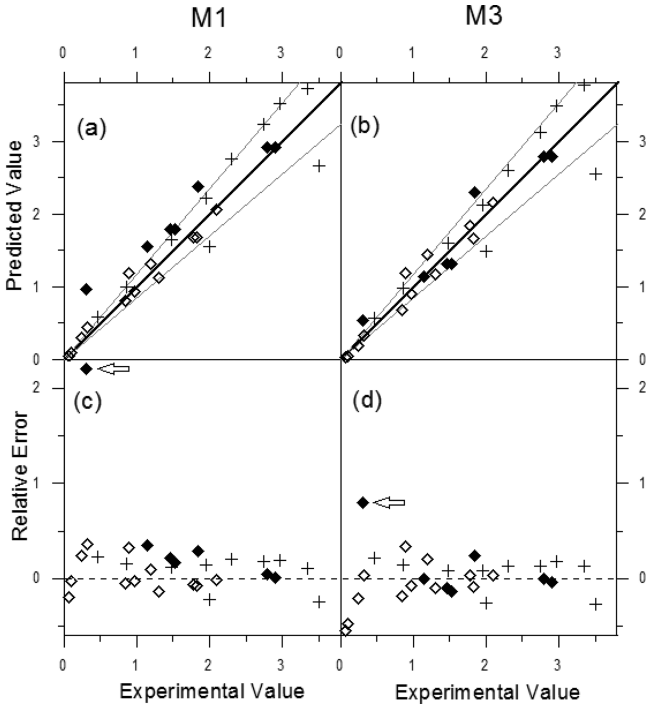

Figure 3. Error analysis of M1 and M3 for lower values. Graphs for M1 are on the left and graphs for M3 on the right. The experimental value and the predicted value represent either the absolute effector concentration (micromolar) or the ratio between effector concentration (micromolar) and protein concentration (micromolar). In graphs a and b, the thick black line represents zero error while the gray lines correspond to ±15% error. Graphs c and d represent the corresponding relative errors, calculated by eq 8. The dashed line in graphs c and d corresponds to zero error. Symbols: (+) ATP second validation data, (◇) ATP/PII second validation data, and (◆) ADP/PII second validation data. The arrows in graphs c and d indicate the largest relative errors of the models.

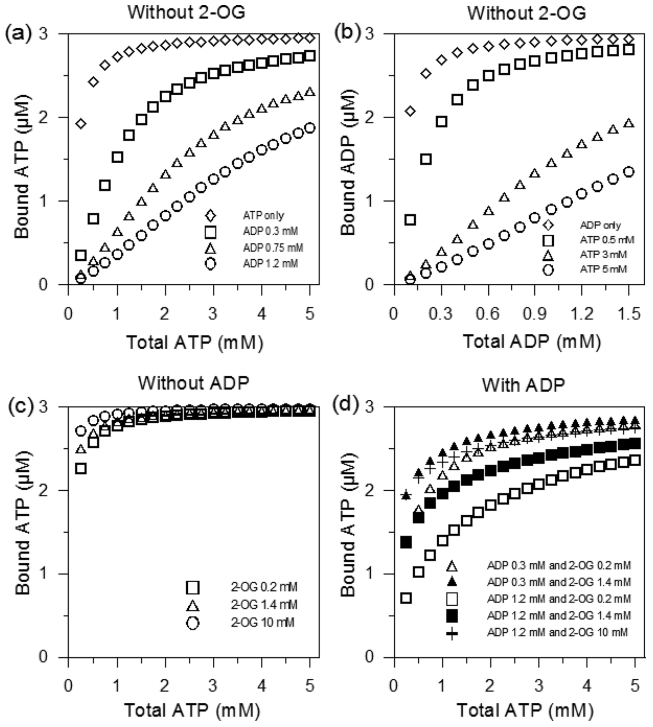

Figure 4. Bound ATP or ADP predicted by M3 as a function of total ATP or ADP concentration under different conditions. The GlnB concentration is 1 μM, which means that the concentration of ATP/ADP binding sites is 3 μM.

Predictions of the GlnB Binding States and Regulation of ATase. Apart from the regulation exerted by the PII effectors, *E. coli* GlnB is also subjected to a reversible posttranslational modification cycle: GlnB is uridylylated under nitrogen limitation conditions and rapidly deuridylylated when the nitrogen level increases.[32]

Even though our model does not describe uridylylation, it can still be used to predict how the fluctuations of ATP, ADP, and 2-OG would affect the activity of protein targets that interact with nonuridylylated GlnB. For example, when the cellular nitrogen levels are high, nonuridylylated GlnB interacts with ATase, promoting its AT activity and inhibiting its AR activity; as a result, GS is inactivated by adenylylation. Nonuridylylated GlnB stimulates AT activity when it has only a single bound 2-OG per trimer or when it has at least one bound ADP per trimer.[4] We used M3 to calculate the proportions of these two GlnB fractions as functions of ATP, ADP, and 2-OG concentrations.

Fraction of GlnB with a Single Bound 2-OG. The fraction of GlnB with a single bound 2-OG is given by the sum of states PTG, PT_2G, PT_3G, PTGD, $PTGD_2$, and PT_2GD (Figure 1); henceforth, we will refer to these states as "GlnB−G states". In the presence of low concentrations of ADP (0.3 mM) and 2-OG (0.1 mM), the greater part of GlnB will be in GlnB−G states for a wide range of ATP concentrations (Figure 5a). As the 2-OG concentration is increased to 1.4 mM and then to 10 mM (graphs c and e of Figure 5, respectively), the fraction of GlnB−G states greatly decreases and the GlnB states with two or three bound 2-OG molecules prevail. When these simulations are repeated at a high ADP concentration of 1.2 mM, the behavior is similar, in the sense that the curves in graphs b, d, and f of Figure 5 for the states with different numbers of bound 2-OG molecules are similar to those in graphs a, c, and e of Figure 5, especially at higher ATP concentrations.

We also calculated the dependence of the proportion of GlnB−G states on the total concentrations of nucleotides and on the ATP:ADP ratio. The total concentration of "ADP + ATP" does not have a significant effect on the proportion of GlnB−G states, this being true at 2-OG concentrations of both 0.1 and 1.4 mM (Figure S1 of the Supporting Information). Conversely, the ATP:ADP ratio has a significant effect on the proportion of GlnB−G states, especially at 2-OG concentrations between 0.3 and 5 mM: the lower the ATP:ADP ratio, the higher the proportion of GlnB−G states (Figure 6). However, at the extremes of the physiological 2-OG range, 0.1 and 10 mM, the absolute proportions of the GlnB−G states are only slightly affected by the ATP:ADP ratio (Figure 6). These results indicate that the fraction of GlnB−G states responds to both 2-OG and the ATP:ADP ratio; however, the response to the ATP:ADP ratio is limited at the extremes of the reported physiological range of 2-OG.

Fraction of GlnB with at Least One Bound ADP. The fraction of GlnB bound to at least one ADP is given by the sum of states PD, PD_2, PD_3, PTD, PT_2D, PTD_2, PTGD, $PTGD_2$, PT_2GD, and PT_2G_2D (Figure 1); henceforth, we will refer to these states as "GlnB−D_{1-3} states". As expected, the fraction of GlnB−D_{1-3} states decreases with an increasing ATP concentration, with this occurring at both low (0.3 mM) and high (3

dx.doi.org/10.1021/bi301659r | *Biochemistry* 2013, 52, 2683−2693

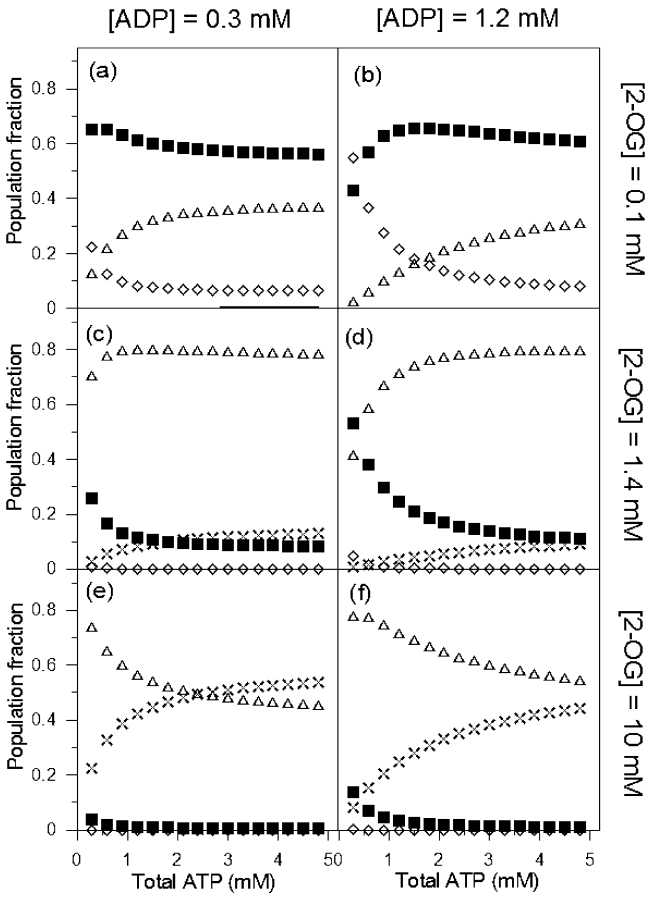

Figure 5. Predictions of M3 about how the fractions of the GlnB populations with different numbers of bound 2-OG molecules vary as a function of the total ATP concentration. The graphs are plotted with different ADP and 2-OG concentrations as indicated. Symbols: (◇) sum of all states without bound 2-OG, (■) sum of all states with a single bound 2-OG (i.e., GlnB−G states), (△) sum of all states with two bound 2-OG molecules, and (×) sum of all states with three bound 2-OG molecules. The GlnB concentration is 1 μM.

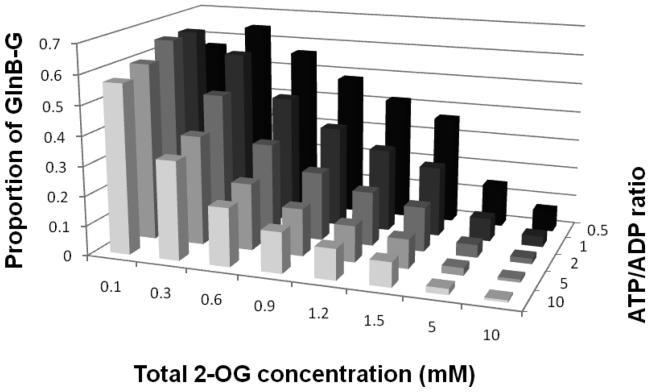

Figure 6. Predictions of M3 about the effect of the ATP:ADP ratio on the proportion of GlnB−G states, plotted for several different 2-OG concentrations. The GlnB−G states are those that contain only one bound 2-OG molecule and are able to promote the AT activity of ATase and the phosphatase activity of NtrB. The GlnB concentration is 1 μM.

mM) ADP concentrations (Figure 7). The total nucleotide concentration does not significantly affect the proportion of the GlnB−D_{1-3} states at a 2-OG concentration of either 0.1 or 1.4

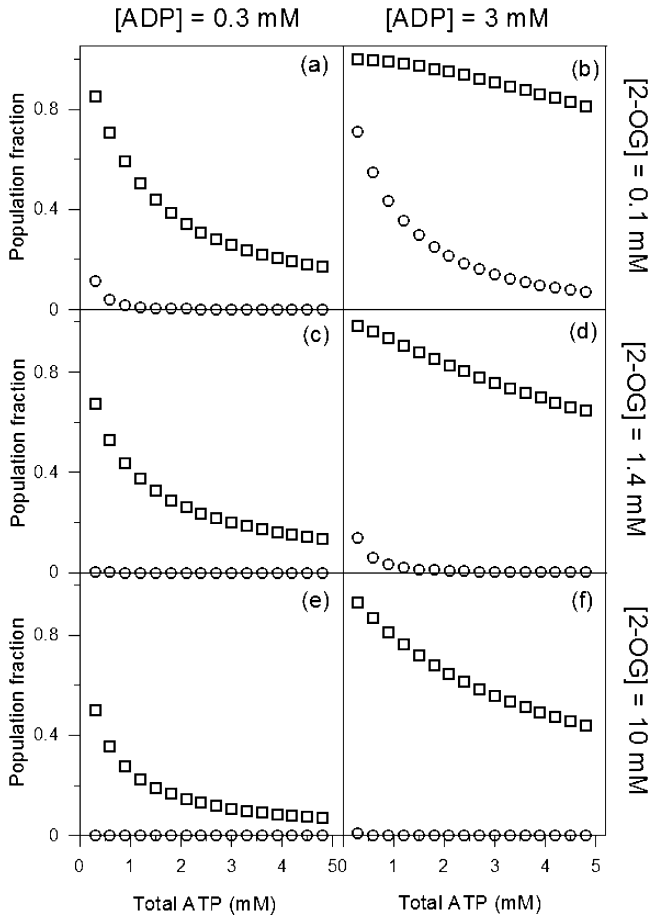

Figure 7. Predictions of M3 about how the fractions of the GlnB−D_{1-3} and GlnB−D_3 populations at different ADP and 2-OG concentrations vary as a function of the total ATP concentration. The graphs are plotted with different ADP and 2-OG concentrations as indicated. Symbols: (□) GlnB−D_{1-3} states and (○) GlnB−D_3 states. The GlnB concentration is 1 μM.

mM (Figure S2 of the Supporting Information). However, reducing the ATP:ADP ratio increases the proportion of the GlnB−D_{1-3} states (Figure 8). Interestingly, changes in the 2-OG concentration have a relatively minor effect on the proportion of the GlnB−D_{1-3} states, with this proportion

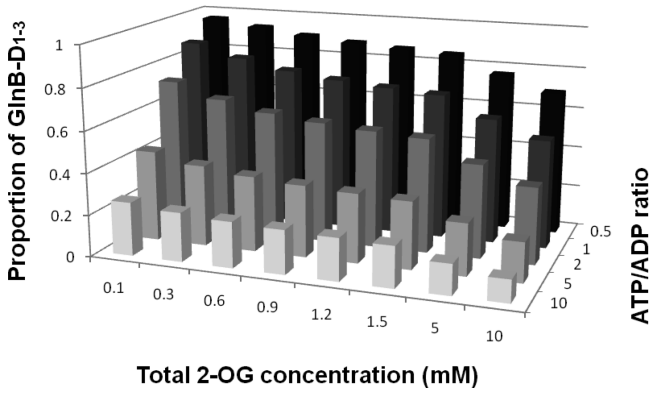

Figure 8. Predictions of M3 about the effect of the ATP:ADP ratio on the proportion of GlnB−D_{1-3} states, plotted for several different 2-OG concentrations. The GlnB−D_{1-3} states are those that contain at least one bound ADP molecule. The GlnB concentration is 1 μM.

dx.doi.org/10.1021/bi301659r | *Biochemistry* 2013, 52, 2683−2693

being reduced significantly only at relatively high 2-OG concentrations (5 and 10 mM) (Figure 8). Hence, the proportion of GlnB−D_{1-3} states is very responsive to the ATP:ADP ratio but only slightly to the 2-OG levels.

Sum of GlnB Fractions GlnB−G and GlnB−D_{1-3}. To analyze the impact of the GlnB effectors on the regulation of the AT activity of ATase, we summed the two GlnB fractions that promote AT activity (i.e., GlnB−G + GlnB−D_{1-3}, but taking care to sum the common states once only); henceforth, we will refer to these states as "GlnB-AT states". The total nucleotide concentration does not significantly affect the proportion of GlnB-AT states (Figure S3 of the Supporting Information). On the other hand, decreases in both the ATP:ADP ratio and the 2-OG concentration increase the proportion of GlnB-AT significantly (Figure 9). Hence, our model suggests that inactivation of GS by the ATase−GlnB complex will be maximized when both the energy (ATP:ADP ratio) and the 2-OG concentration are low.

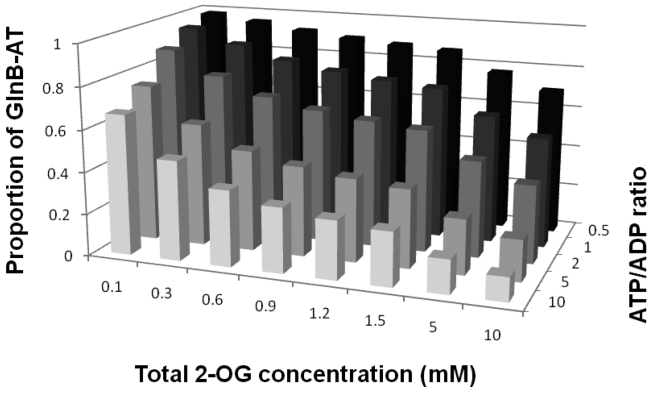

Figure 9. Predictions of M3 about the effect of the ATP:ADP ratio on the proportion of GlnB-AT states, plotted for several different 2-OG concentrations. The GlnB-AT states are those that contain only one bound 2-OG molecule or at least one bound ADP molecule. The GlnB concentration is 1 μM.

DISCUSSION

Main Contribution of This Work. We have demonstrated an approach to modeling PII that can integrate a set of binding rules into a single model capable of describing the binding states of PII when ATP, ADP, and 2-OG are present simultaneously. This approach is not new: it has its roots in the landmark paper of Monod et al.[33] about modeling allosteric interactions, although it has not previously been applied to PII. The advantage of this approach is its ability to incorporate different hypotheses and experimental evidence about the rules governing the binding of effectors. This flexibility is demonstrated by the fact that we proposed four different models, based on various suggestions that have been made in the literature about the binding of effectors to PII. Current models[6,17] do not have this flexibility.

It is important to realize that it is not necessarily the case that any one of the four models proposed in this work is a correct representation of the rules that govern the binding of effectors to GlnB of *E. coli*. Future experimental evidence may lead to the proposal of a different set of binding rules. However, once these rules are established, the approach to modeling that we have demonstrated can be applied to arrive at an appropriate model. Of course, this approach could also be applied to GlnK, the paralogue of GlnB, and to PII proteins from other organisms. The establishment of appropriate binding rules for other PII proteins would require a significant amount of experimental work, similar to that conducted by Jiang and Ninfa[6] and listed in Table S3 of the Supporting Information. In such work, to have a more stringent test for the fitting of the model and estimation of dissociation constants, it would be interesting to determine the concentrations of all bound effectors in those experiments in which more than one effector were present.

Comparison of our Modeling Approach with That of Jiang and Ninfa. Jiang and Ninfa[6] used the following equation to describe the binding of ligands to PII:

$$[X]_B = [[P]_T(K_{X2}K_{X3}[X] + 2K_{X3}[X]^2 + 3[X]^3)] / (K_{X1}K_{X2}K_{X3} + K_{X2}K_{X3}[X] + K_{X3}[X]^2 + [X]^3) \quad (8)$$

where $[X]_B$ is the bound ligand concentration and K_{X1}, K_{X2}, and K_{X3} are the dissociation constants associated with the binding of the first, second, and third ligand molecules, respectively.

This equation is correct for describing the binding of a single effector to a protein with two or three classes of sites (when used to describe only two classes of sites, K_{X2} and K_{X3} are set equal[6]): Our models simplify to give eq 8 when only a single effector is present. When eq 8 is adjusted to binding data obtained in experiments involving only a single effector (i.e., "ATP only" or "ADP only"), then K_{X1}, K_{X2}, and K_{X3} represent the true dissociation constants, in the sense that they represent the dissociation constants of the corresponding dissociation reactions proposed in the reaction scheme.

On the other hand, when more than one effector is present, care must be taken in interpreting the results of fitting eq 8 to experimental data: When ATP and 2-OG are present, then K_{X1}, K_{X2}, and K_{X3} in eq 8 are apparent constants. If the equation is used to describe bound ATP, then K_{X1}, K_{X2}, and K_{X3} will be functions of the free 2-OG concentration. If the equation is used to describe bound 2-OG, then K_{X1}, K_{X2}, and K_{X3} will be functions of the free ATP concentration.

For example, Jiang and Ninfa[6] conducted an experiment in which the quantity of bound 2-OG was determined as a function of the free 2-OG concentration, in experiments in which the concentration of added ATP was kept at 4 mM. In the absence of ADP, M4 (or M3, putting $K_{T2} = K_{T3}$) simplifies to give an equation for the binding of 2-OG that has a mathematical form equal to that of eq 8, with the following equivalencies:

$$K_{X1} = K_{G1} \times \frac{1 + \frac{[T]}{K_{T1}} + \frac{[T]^2}{K_{T1}K_{T2}} + \frac{[T]^3}{K_{T1}K_{T2}K_{T3}}}{\frac{[T]}{K_{T1}} + \frac{[T]^2}{K_{T1}K_{T2}} + \frac{[T]^3}{K_{T1}K_{T2}K_{T3}}} \quad (9a)$$

$$K_{X2} = K_{G2} \times \frac{1 + \frac{[T]}{K_{T2}} + \frac{[T]^2}{K_{T2}K_{T3}}}{\frac{[T]}{K_{T2}} + \frac{[T]^2}{K_{T2}K_{T3}}} \quad (9b)$$

$$K_{X3} = K_{G3}\frac{1 + \frac{[T]}{K_{T3}}}{\frac{[T]}{K_{T3}}} \quad (9c)$$

In other words, for this kind of experiment, K_{X1}, K_{X2}, and K_{X3} in eq 8 do not represent the true dissociation constants for 2-OG. Rather, they represent combinations of the true dissociation constants and terms that are functions of the ATP concentration used. Of course, if care is taken to use an

ATP concentration that is significantly larger than K_{T3}, as Jiang and Ninfa[6] did, then the values of K_{X1}, K_{X2}, and K_{X3} will be close to the true values of K_{G1}, K_{G2}, and K_{G3}. If experiments are conducted at lower ATP concentrations, then this will not be the case.

It Is Possible for 2-OG To Favor ATP Binding without Necessarily Affecting the Affinity of PII for ATP. As pointed out in the Results, M3 is able to describe the fact that 2-OG enhances the binding of ATP, even though in M3 the affinity of PII for ATP is not affected by the presence of 2-OG (i.e., the values of K_{T1}, K_{T2}, and K_{T3} are independent of the concentration of 2-OG). In the absence of ADP, M3 (i.e., $K_{T2} = K_{T3}$) simplifies to give an equation for the binding of ATP that has a mathematical form equal to that of eq 8, with the following equivalencies:

$$K_{X1} = K_{T1}\frac{1}{1 + \frac{[G]}{K_{G1}}} \tag{10a}$$

$$K_{X2} = K_{T2} \times \frac{1 + \frac{[G]}{K_{G1}}}{1 + \frac{[G]}{K_{G1}} + \frac{[G]^2}{K_{G1}K_{G2}}} \tag{10b}$$

$$K_{X3} = K_{T3} \times \frac{1 + \frac{[G]}{K_{G1}} + \frac{[G]^2}{K_{G1}K_{G2}}}{1 + \frac{[G]}{K_{G1}} + \frac{[G]^2}{K_{G1}K_{G2}} + \frac{[G]^3}{K_{G1}K_{G2}K_{G3}}} \tag{10c}$$

In other words, for an experiment in which the concentration of ATP is varied while the concentration of added 2-OG is kept constant, K_{X1}, K_{X2}, and K_{X3} in eq 8 do not represent the true dissociation constants for ATP. Rather, they represent combinations of the true dissociation constants and terms that are functions of the 2-OG concentration used. This could explain why Jiang and Ninfa[6] reported different sets of K_d values through the application of eq 8 to data from ATP binding experiments undertaken in the presence of different concentrations of 2-OG, with the apparent affinity increasing with an increasing 2-OG concentration. M3 is able to explain this phenomenon: Figure 10 shows how the apparent dissociation constants for ATP, as expressed by eqs 10a–10c, decrease with an increasing concentration of 2-OG, suggesting a higher affinity. However, it must be remembered that K_{T1}, K_{T2}, and K_{T3} are held constant in the plotting of this figure.

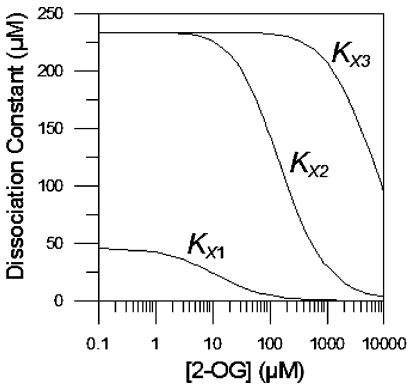

Figure 10. Effect of the free 2-OG concentration on the apparent dissociation constants for ATP. The values of K_{X1}, K_{X2}, and K_{X3} that would be obtained through use of eq 8 to analyze data (for a varying ATP concentration and a constant 2-OG concentration) were obtained by substituting the values presented in Table 1 for K_{T1}, K_{T2}, K_{T3}, K_{G1}, K_{G2}, and K_{G3} for M3 into eqs 10a–10c.

The conclusion from this analysis is that it is possible for the binding of ATP to be enhanced by the presence of 2-OG, without it being necessary to invoke a decrease in the dissociation constants for ATP itself to explain this phenomenon.

Insights into PII Signaling Behavior. Jiang and Ninfa[4] proposed a scheme of 56 hypothetical binding states, with 2-OG being allowed to bind to a subunit without any bound nucleotide and to a subunit with a bound ADP. Figure 1 differs significantly in that it allows 2-OG to bind only to a subunit that has a bound ATP, thereby eliminating 36 of the hypothetical states that they proposed.[4] Structural studies are required to elucidate which binding states are in fact possible. On the other hand, our simulations with M3 are consistent with the hypotheses raised by Jiang and Ninfa[4] about *E. coli* GlnB that (1) GlnB is able to bind ATP and ADP simultaneously to the same trimer, (2) under physiological conditions the GlnB trimer will have all three of its nucleotide binding sites occupied (i.e., by ATP or ADP), and (3) 2-OG antagonizes the binding of ADP to GlnB by favoring the binding of the competing nucleotide ATP.

Jiang and Ninfa[6] obtained a good fit to binding data obtained with ATP as the only ligand by using a model with two classes of binding sites for ATP (i.e., $K_{X2} = K_{X3}$ in eq 6). Because in our work M3, which also considers two classes of binding sites for ATP, also showed good results, we hypothesize that the binding of the first nucleotide molecule changes the GlnB conformation, making it harder for further nucleotide molecules to bind. Confirmation of our hypothesis would require the determination of GlnB structures with one, two, and three nucleotide molecules bound per GlnB trimer.

Interestingly, our simulations suggest that GlnB trimers with three bound ADP molecules are very unlikely to accumulate under normal physiological conditions (Figure 7). This allows a possible insight into why GlnK, rather than GlnB, was selected to regulate the activity of the ammonium transporter AmtB. Because the AmtB–PII interaction is stabilized (inactivating the transport of ammonium by AmtB) when the PII trimer is occupied by three ADP molecules,[5,34,35] GlnB would not be appropriate for interacting with AmtB. We suggest that GlnK must have a higher affinity for ADP, such that the GlnK state with three bound ADP molecules would accumulate under the appropriate physiological conditions.

Our simulations of the various binding states of GlnB lead us to hypothesize about why both the GlnB–G states and the GlnB–D_{1-3} states were selected to regulate the AT activity during evolution. Alone, neither the GlnB–G states nor the GlnB–D_{1-3} states give a well-modulated response to fluctuations in the 2-OG concentration and the ATP:ADP ratio. On the contrary, the combination of these states (i.e., the GlnB-AT states) varies significantly over the whole physiological range of these two signals. Hence, ammonium assimilation through GS will be limited not only by the availability of carbon in the form of 2-OG but also by the availability of cellular energy, sensed as the ATP:ADP ratio. These results support the hypothesis that has been raised previously by various authors that the PII proteins can act not only as 2-OG sensors but also as ATP/ADP sensors.[4,6,9,36]

dx.doi.org/10.1021/bi301659r | *Biochemistry* 2013, 52, 2683–2693

■ ASSOCIATED CONTENT

Supporting Information

Additional results. This material is available free of charge via the Internet at http://pubs.acs.org.

■ AUTHOR INFORMATION

Corresponding Author

*Phone: +55-41-33611536. Fax: +55-41-32662042. E-mail: davidmitchell@ufpr.br.

Present Address

§F.d.C.: Departamento de Engenharia Química, Universidade Federal de Santa Maria, Avenida Roraima, 1000, Santa Maria 97105-900, Rio Grande do Sul, Brazil.

Funding

This work was supported by the Brazilian Program of National Institutes of Science and Technology-INCT/Brazilian Research Council-CNPq/MCT. Research scholarships were granted to R.A.d.R. and T.A.W. by CAPES (Coordenação de Aperfeiçoamento de Pessoal de Nivel Superior), a Brazilian government agency for the development of scientific personnel, and to F.d.C., E.M.d.S., L.F.H., and D.A.M. by CNPq (Conselho Nacional de Desenvolvimento Científico e Tecnológico), a Brazilian government agency for the advancement of science.

Notes

The authors declare no competing financial interest.

■ ABBREVIATIONS

2-OG, 2-oxoglutarate; K_d, dissociation constant; GS, glutamine synthetase; ATase, adenylyltransferase/adenylyl-removing enzyme; AT, adenylyltransferase; AR, adenylyl-removing; PSO, particle swarm optimization.

■ REFERENCES

(1) Huergo, L. F., Chandra, G., and Merrick, M. (2013) P(II) signal transduction proteins: Nitrogen regulation and beyond. *FEMS Microbiol. Rev. 37*, 251−283.

(2) Xu, Y., Carr, P. D., Huber, T., Vasudevan, S. G., and Ollis, D. L. (2001) The structure of the PII-ATP complex. *Eur. J. Biochem. 268*, 2028−2037.

(3) Xu, Y., Cheah, E., Carr, P. D., van Heeswijk, W. C., Westerhoff, H. V., Vasudevan, S. G., and Ollis, D. L. (1998) GlnK, a PII-homologue: Structure reveals ATP binding site and indicates how the T-loops may be involved in molecular recognition. *J. Mol. Biol. 282*, 149−165.

(4) Jiang, P., and Ninfa, A. J. (2009) Sensation and signaling of α-ketoglutarate and adenylylate energy charge by the *Escherichia coli* PII signal transduction protein require cooperation of the three ligand-binding sites within the PII trimer. *Biochemistry 48*, 11522−11531.

(5) Conroy, M. J., Durand, A., Lupo, D., Li, X. D., Bullough, P. A., Winkler, F. K., and Merrick, M. (2007) The crystal structure of the *Escherichia coli* AmtB-GlnK complex reveals how GlnK regulates the ammonia channel. *Proc. Natl. Acad. Sci. U.S.A. 104*, 1213−1218.

(6) Jiang, P., and Ninfa, A. J. (2007) *Escherichia coli* PII signal transduction protein controlling nitrogen assimilation acts as a sensor of adenylate energy charge *in vitro*. *Biochemistry 46*, 12979−12996.

(7) Fokina, O., Chellamuthu, V. R., Forchhammer, K., and Zeth, K. (2010) Mechanism of 2-oxoglutarate signaling by the *Synechococcus elongatus* PII signal transduction protein. *Proc. Natl. Acad. Sci. U.S.A. 107*, 19760−19765.

(8) Maier, S., Schleberger, P., Lu, W., Wacker, T., Pfluger, T., Litz, C., and Andrade, S. L. (2011) Mechanism of disruption of the Amt-GlnK complex by P(II)-mediated sensing of 2-oxoglutarate. *PLoS One 6* (10), e26327.

(9) Gerhardt, E. C., Araujo, L. M., Ribeiro, R. R., Chubatsu, L. S., Scarduelli, M., Rodrigues, T. E., et al. (2012) Influence of the ADP/ATP ratio, 2-oxoglutarate and divalent ions on *Azospirillum brasilense* PII protein signaling. *Microbiology 158*, 1656−1663.

(10) Truan, D., Huergo, L. F., Chubatsu, L. S., Merrick, M., Li, X. D., and Winkler, F. K. (2010) A new P(II) protein structure identifies the 2-oxoglutarate binding site. *J. Mol. Biol. 400*, 531−539.

(11) van Heeswijk, W. C., Hoving, S., Molenaar, D., Stegeman, B., Kahn, D., and Westerhoff, H. V. (1996) An alternative P_{II} protein in the regulation of glutamine synthetase in *Escherichia coli*. *Mol. Microbiol. 21*, 133−146.

(12) van Heeswijk, W. C., Wen, D., Clancy, P., Jaggi, R., Ollis, D. L., Westerhoff, H. V., and Vasudevan, S. G. (2000) The *Escherichia coli* signal transducers PII (GlnB) and GlnK form heterotrimers *in vivo*: Fine tuning the nitrogen signal cascade. *Proc. Natl. Acad. Sci. U.S.A. 97*, 3942−3947.

(13) Atkinson, M., and Ninfa, A. J. (1999) Characterization of the GlnK protein of *Escherichia coli*. *Mol. Microbiol. 32*, 301−313.

(14) Atkinson, M. R., and Ninfa, A. J. (1998) Role of the GlnK signal transduction protein in the regulation of nitrogen assimilation in *Escherichia coli*. *Mol. Microbiol. 29*, 431−447.

(15) Thomas, G., Coutts, G., and Merrick, M. (2000) The *glnKamtB* operon: A conserved gene pair in prokaryotes. *Trends Genet. 16*, 11−14.

(16) Radchenko, M. V., Thornton, J., and Merrick, M. (2010) Control of AmtB-GlnK complex formation by intracellular levels of ATP, ADP and 2-oxoglutarate. *J. Biol. Chem. 285*, 31037−31045.

(17) Bruggeman, F. J., Boogerd, F. C., and Westerhoff, H. V. (2005) The multifarious short-term regulation of ammonium assimilation of *Escherichia coli*: Dissection using an *in silico* replica. *FEBS J. 272*, 1965−1985.

(18) Suzuki, K., and Post, R. L. (1997) Equilibrium of phosphointermediates of sodium and potassium ion transport adenosine triphosphatase. *J. Gen. Physiol. 109*, 537−554.

(19) Sutendra, G., Wong, S., Fraser, M. E., and Huber, R. E. (2007) β-Galactosidase (*Escherichia coli*) has a second catalytically important Mg^{2+} site. *Biochem. Biophys. Res. Commun. 352*, 566−570.

(20) Kamberov, E. S., Atkinson, M. R., and Ninfa, A. J. (1995) The *Escherichia coli* PII signal transduction protein is activated upon binding 2-ketoglutarate and ATP. *J. Biol. Chem. 270*, 17797−17807.

(21) Eberhart, R., and Kennedy, J. (1995) A new optimizer using particle swarm theory. *Proceedings of the sixth international symposium on micro machine and human science*, Nagoya, Japan, pp 39−43.

(22) Kennedy, J., and Eberhart, R. (1995) Particle swarm optimization. *Proceedings of the IEEE International Conference on the Neural Network*, pp 1942−1948, IEEE, Piscataway, NJ.

(23) El-Naggar, K. M., AlRashidi, M. R., and Al-Othman, A. K. (2009) Estimating the input-output parameters of thermal plants using PSO. *Energy Convers. Manage. 50*, 1767−1772.

(24) van den Bergh, F., and Engelbrecht, A. P. (2006) A study of particle swarm optimization particle trajectories. *Inf. Sci. 176*, 937−971.

(25) Press, W. H., Teukolsky, S. A., Vetterling, W. T., and Flannery, B. P. (1992) *Numerical recipes in Fortan 77. The art of scientific computing*, 2nd ed., Vol. *1*, Press Syndicate of the University of Cambridge, New York.

(26) Schneider, D. A., and Gourse, R. L. (2003) Relationship between Growth Rate and ATP Concentration in *Escherichia coli*. *J. Biol. Chem. 279*, 8262−8268.

(27) Gigliobianco, T., Lakaye, B., Wins, P., Moualij, B. E., Zorzi, W., and Bettendorff, L. (2010) Adenosine thiamine triphosphate accumulates in *Escherichia coli* cells in response to specific conditions of metabolic stress. *BMC Microbiol. 10*, 148.

(28) Rozkov, A., and Enfors, S. O. (1998) Stabilization of a proteolytically sensitive cytoplasmatic recombinant protein during transition to downstream processing. *Biotechnol. Bioeng. 62*, 730−738.

(29) Senior, P. J. (1975) Regulation of nitrogen metabolism in *Escherichia coli* and *Klebsiella aerogenes*: Studies with the continuous-culture technique. *J. Bacteriol. 123*, 407−418.

(30) Yuan, J., Doucette, C. D., Fowler, W. U., Feng, X. J., Piazza, M., Rabitz, H. A., Wingreen, N. S., and Rabinowitz, J. D. (2009) Metabolomics-driven quantitative analysis of ammonia assimilation in *E. coli*. *Mol. Syst. Biol. 5*, 302.
(31) Ma, H., Boogerd, F. C., and Goryanin, I. (2009) Modelling nitrogen assimilation of *Escherichia coli* at low ammonium concentration. *J. Biotechnol. 144*, 175−183.
(32) Jiang, P., Peliska, J. A., and Ninfa, A. J. (1998) Enzymological characterization of the signal-transducing uridylyltransferase/uridylyl-removing enzyme (EC 2.7.7.59) of *Escherichia coli* and its interaction with the PII protein. *Biochemistry 37*, 12782−12794.
(33) Monod, J., Wyman, J., and Changeux, J. (1965) On the nature of allosteric transitions: A plausible model. *J. Mol. Biol. 12*, 88−118.
(34) Gruswitz, F., O'Connell, J., III, and Stroud, R. M. (2007) Inhibitory complex of the transmembrane ammonia channel, AmtB, and the cytosolic regulatory protein, GlnK, at 1.96 Å. *Proc. Natl. Acad. Sci. U.S.A. 104*, 42−47.
(35) Rodrigues, T. E., Souza, V. E., Monteiro, R. A., Gerhardt, E. C., Araujo, L. M., Chubatsu, L. S., et al. (2011) *In vitro* interaction between the ammonium transport protein AmtB and partially uridylylated forms of the P(II) protein GlnZ. *Biochim. Biophys. Acta 1814*, 1203−1209.
(36) Fokina, O., Herrmann, C., and Forchhammer, K. (2011) Signal-transduction protein PII from *Synechococcus elongatus* PCC 7942 senses low adenylate energy charge *in vitro*. *Biochem. J. 440*, 147−156.